



Ferromagnetic properties of (Ga,Mn)N nanowires grown by a chemical vapor deposition method

Jeong Min Baik and Jong-Lam Lee

Citation: *Journal of Vacuum Science & Technology B* **23**, 530 (2005); doi: 10.1116/1.1880212

View online: <http://dx.doi.org/10.1116/1.1880212>

View Table of Contents: <http://scitation.aip.org/content/avs/journal/jvstb/23/2?ver=pdfcov>

Published by the AVS: Science & Technology of Materials, Interfaces, and Processing

Articles you may be interested in

Defect states of chemical vapor deposition grown GaN nanowires: Effects and mechanisms in the relaxation of carriers

J. Appl. Phys. **106**, 054311 (2009); 10.1063/1.3212989

Doping concentration dependence of ferromagnetic ordering in (Ga,Mn)N nanowires

Appl. Phys. Lett. **89**, 173117 (2006); 10.1063/1.2364882

Fabrication of (Ga,Mn)N nanowires with room temperature ferromagnetism using nitrogen plasma

Appl. Phys. Lett. **87**, 042105 (2005); 10.1063/1.1999862

Ferromagnetic Mn-doped GaN nanowires

Appl. Phys. Lett. **86**, 032506 (2005); 10.1063/1.1852725

Origin of high-temperature ferromagnetism in (Ga,Mn)N layers grown on 4H-SiC(0001) by reactive molecular-beam epitaxy

Appl. Phys. Lett. **82**, 2077 (2003); 10.1063/1.1564292



Instruments for Advanced Science

Contact Hiden Analytical for further details:

W www.HidenAnalytical.com

E info@hiden.co.uk

CLICK TO VIEW our product catalogue



Gas Analysis

- › dynamic measurement of reaction gas streams
- › catalysis and thermal analysis
- › molecular beam studies
- › dissolved species probes
- › fermentation, environmental and ecological studies



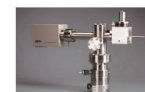
Surface Science

- › UHV TPD
- › SIMS
- › end point detection in ion beam etch
- › elemental imaging - surface mapping



Plasma Diagnostics

- › plasma source characterization
- › etch and deposition process reaction
- › kinetic studies
- › analysis of neutral and radical species



Vacuum Analysis

- › partial pressure measurement and control of process gases
- › reactive sputter process control
- › vacuum diagnostics
- › vacuum coating process monitoring

Ferromagnetic properties of (Ga,Mn)N nanowires grown by a chemical vapor deposition method

Jeong Min Baik and Jong-Lam Lee^{a)}

Department of Materials Science and Engineering, Pohang University of Science and Technology, Pohang, Kyungbuk 790-784, Korea

(Received 27 September 2004; accepted 31 January 2005; published 18 March 2005)

Ferromagnetic (Ga,Mn)N nanowires were grown on sapphire substrates at 900 °C by a chemical vapor deposition. Synchrotron radiation photoemission spectroscopy revealed that no secondary phases were found in the grown nanowire, meaning the dissolution of Mn atoms to form a solid solution in GaN nanowire. Fermi level was apart by 3.0 eV in the GaN nanowire (*n*-type), and it shifted toward the valance band maximum with ammonia flow rate. The Ga-to-N ratio decreased with the increase of ammonia flow rate, leading to the increase of Ga vacancies. From this, it is suggested that both increases in magnetic moment and Curie temperature with ammonia flow rate originated from the solid solution of Mn and Ga vacancies. © 2005 American Vacuum Society. [DOI: 10.1116/1.1880212]

I. INTRODUCTION

Diluted magnetic semiconductors (DMS's) based on III-V semiconductors such as GaAs and GaN can be fabricated by incorporating a high concentration of magnetic ions into III-V semiconductors by molecular-beam epitaxy (MBE) or ion implantation.¹⁻⁴ It was theoretically suggested that (Ga,Mn)N films with a high Mn concentration (~5 at. %) and a high hole concentration (~10²⁰ cm⁻³) could yield a high Curie temperature T_c (≥ 300 K).⁵ This allows spintronic devices to be operated at room temperature. Recently, a Mn-doped GaN film showing ferromagnetic behavior above room temperature was successfully grown on sapphire (0001) by MBE.⁴ The ferromagnetic property was also achieved by implanting Mn ions into GaN and subsequent annealing.³ Most of the work to obtain ferromagnetic properties has focused on the microcrystalline,² bulk,⁶ epitaxial,⁴ Mn-implanted,³ and Mn-diffused (Ga,Mn)N.⁷ However, no results on ferromagnetic properties of nanometer-sized (Ga,Mn)N materials have been reported.

There has been research which discusses the origin of ferromagnetic properties in (Ga,Mn)N semiconductor. It was proposed that the ferromagnetic properties might be due to the solid solution of (Ga,Mn)N,^{4,7} while the secondary phases such as Ga-Mn and Mn-N compounds could be origin of ferromagnetism.³ A number of competing theoretical models⁸⁻¹⁰ for (Ga,Mn)N including the mean-field Zener model⁵ were also developed. Despite a number of works mentioned above, however no works on origin of ferromagnetic properties in nanosized DMS's were investigated.

In this work, we study magnetic properties of (Ga,Mn)N nanowires with microstructural change by controlling ammonia flow rate in the growth by chemical vapor deposition. The morphology of nanowires is analyzed using field emission scanning electron microscopy (FESEM) and high resolution transmission electron microscopy (HRTEM). Synchro-

tron x-ray diffraction (XRD) and synchrotron radiation photoemission spectroscopy (SRPES) are employed to identify secondary phases and chemical bonding states in nanowires.

II. EXPERIMENT

A (0001) sapphire substrate was used as a starting substrate. Before the growth of GaN nanowire, the substrate was cleaned with acetone, methanol, and deionized water. A thin layer of 30-Å-thick Au was evaporated to enhance the formation of GaN nanowire.¹¹

A (2:1) mixture by weight of pure Ga and MnCl₂ powders (99.95%) was introduced into the middle of the quartz boat. The quartz boat was then placed in a horizontal furnace, evacuated to 10 mTorr and purged with a constant nitrogen flow of 500 sccm. Then, the furnace temperature was increased to 900 °C. Then, a high purity NH₃ (99.995%) was introduced into the reaction chamber. In order to find the effect of atomic stoichiometry of GaN on ferromagnetic properties of (Ga,Mn)N nanowires, the NH₃ flow rate was changed from 50 to 150 sccm. The reaction was maintained for 2 h under a pressure of 1 atm. After the furnace was cooled to room temperature, a layer of light-yellow products was visible on the surface of the substrate in the quartz boat.

High-resolution XRD and SRPES using synchrotron radiation were carried out at the 3C2 and 8A1 beamlines at Pohang Accelerator Laboratory (PAL), respectively. For high-resolution XRD measurements, the wavelength of incident x ray was set at 1.488 Å by a double bounce Si (111) monochromator. For SRPES measurements, a hemispherical electron energy analyzer with 16 energy-detecting channels/windows was used, and the energy separation/resolution per window was 0.05 eV. An incident photon energy of 700 eV was used for measurement of the core-level spectra of Ga 3*d* and Mn 2*p*. The binding energy of the core-level spectrum was calibrated using the Au 4*f* core level of Au foil. The Fermi level was determined by linearly extrapolating the sloped region with a base line in the valence-band spectrum

^{a)} Author to whom correspondence should be addressed; electronic mail: jlllee@postech.edu

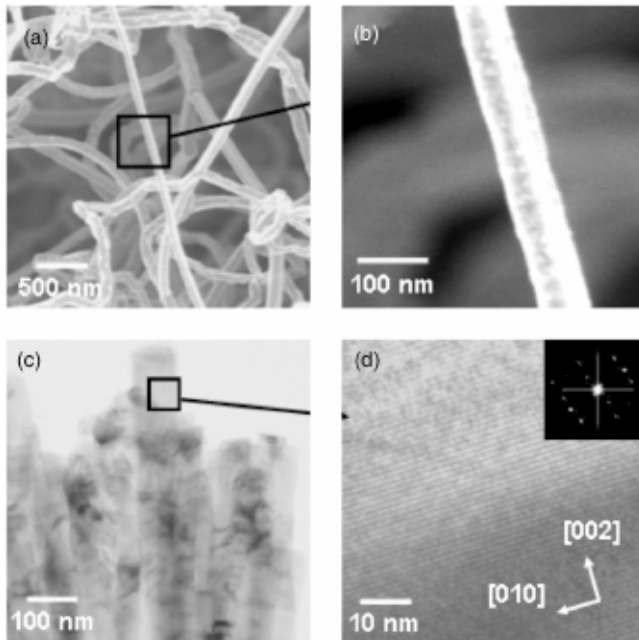


Fig. 1. (a) FESEM image of (Ga,Mn)N nanowires with random orientation. The expanded image of a smaller part in (a) is shown in (b). Cross-sectional TEM image (c) and high-resolution image (d) of (Ga,Mn)N nanowires. Corresponding electron diffraction patterns are also shown in the inset.

of the Au foil. The FESEM with a high spatial resolution of 1.5 nm was used to characterize the morphology of the products. The HRTEM images were collected using a JEOL 2010F operated with 200 KV. Its spatial resolution was 0.19 nm. Magnetization measurement was carried out using a superconducting quantum interference device magnetometer (MPMSXL, Quantum Design Co., Ltd.).

III. RESULTS AND DISCUSSION

Figures 1(a) and 1(b) showed the morphology of (Ga,Mn)N nanowires grown at an ammonia flow rate of 150 sccm. The scanning electron microscopy images revealed that the nanowires exhibited a length of a few micrometers and a mean diameter of 95 nm. The cross-sectional TEM image and high-resolution image of the nanowires were also shown in Figs. 1(c) and 1(d). The selected area electron diffraction (SAED) patterns from a single nanowire confirmed that the nanowire is a single-crystalline wurzite structure. The growth direction of the (Ga,Mn)N nanowire was [002] direction. No Mn-related secondary phases were found in the (Ga,Mn)N nanowires. The microstructure of nanowires such as diameter, length, and SAED patterns were independent of ammonia flow rate.

Figure 2 shows magnetization curves at 10 K for (Ga,Mn)N nanowires as a function of ammonia flow rate. The diamagnetic background of sapphire substrate was subtracted. Hysteresis loops of all samples showed clear ferromagnetic behavior. The ferromagnetic signal became strong with increasing ammonia flow rate. The saturation magnetic moment (M_s) increased from 4.1×10^{-6} to 8.5×10^{-6} emu as the flow rate increased from 50 to 150 sccm. The coercive

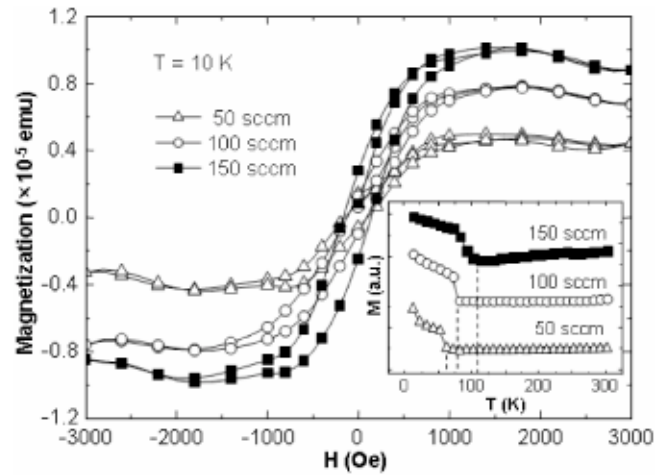


Fig. 2. Magnetization curves at 10 K for (Ga,Mn)N nanowires with ammonia flow rates of 50, 100, and 150 sccm. The temperature dependence of the magnetic moment is plotted in the inset.

field (H_c) also increased to 145 Oe at the flow rate of 150 sccm. Temperature dependence of the magnetic moment is also plotted in the inset of Fig. 2. The T_c showed the highest value (~ 120 K) at an ammonia flow rate of 150 sccm. No superparamagnetic property was observed in the nanowires.

Figure 3 shows XRD profiles of (Ga,Mn)N nanowires with ammonia flow rate. Only two peaks corresponding to GaN (100) and GaN (002) were observed in all samples. In our previous works,¹² nanosized secondary phases such as Mn_3N_2 and $Mn_6N_{2.58}$ were produced in Mn-implanted GaN after annealing at 900 °C. These compounds were observed in XRD measurements, as shown in the inset of Fig. 3. However, no diffraction peaks corresponding to the Mn precipi-

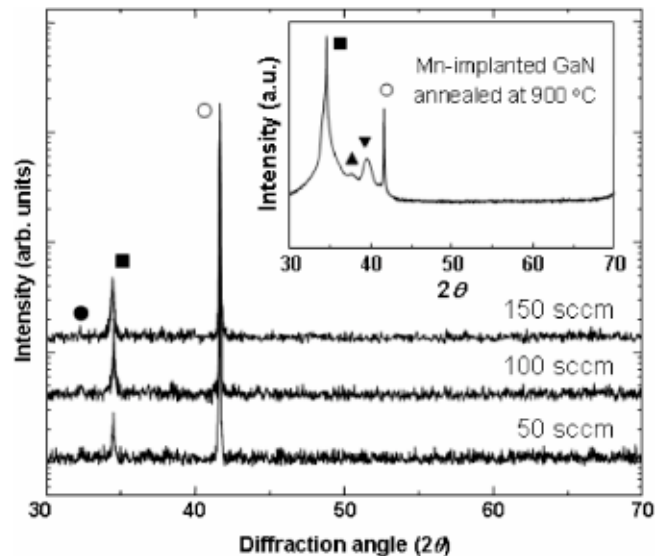


Fig. 3. Change of XRD scans for (Ga,Mn)N nanowires with ammonia flow rate of 50, 100, and 150 sccm. The incident photon energy of 8 keV ($\lambda = 1.55$ Å) was used in the measurements. XRD profile of Mn-implanted GaN annealed at 900 °C is also shown. [●: GaN(100), ■: GaN (002), ○: $Al_2O_3(001)$, ▲: $Mn_3N_2(103)$ ▼: $Mn_6N_{2.58}(002)$].

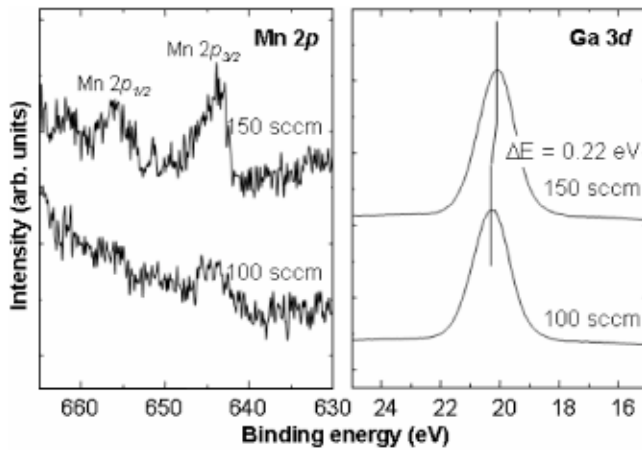


FIG. 4. SRPES spectra of Mn $2p$ and Ga $3d$ core levels for (Ga,Mn)N nanowires with ammonia flow rates of 100 and 150 sccm.

tates or Mn-related secondary phases were observed in the nanowires. This confirmed the formation of solid solution of Mn atoms in GaN nanowires.

Figure 4 displays the SRPES spectra of Ga $3d$ and Mn $2p$ core levels for (Ga,Mn)N nanowires. The peak of Ga $3d$ spectrum shifted about 0.22 eV toward lower binding energies with increasing ammonia flow rate from 100 to 150 sccm, indicating that the Fermi energy level moved toward the valence band maximum (VBM). The relative atomic ratio of Ga-to-N was determined from the atomic concentrations of each element, calculated from the integral peak intensities of Ga $3d$ and N $1s$ spectra, summarized in Table I. The ratio measured at a detection angle of $\theta=90$ deg in GaN nanowire was set to 1.0 for reference. The Ga/N ratio decreased with the increase of ammonia flow rate. This means that the surface of nanowire changed to the Ga-deficient surface with the increase of ammonia flow rate. In the meanwhile, the peak intensities of Mn $2p_{3/2}$ and Mn $2p_{1/2}$ spectra in the Mn $2p$ spectrum increased, indicating that the dissolution of Mn atoms in the nanowires enhanced. No additional chemical bonds due to Mn-related secondary phases were found in Mn $2p$ spectrum, consistent with synchrotron radiation x-ray diffraction results that no secondary phases were observed.

The valence band spectra were shown in Fig. 5. The surface band bending of (Ga,Mn)N nanowires changed with ammonia flow rate. The position of VBM was determined by the kink point given by two solid lines, extracted from the background and straight onset in valence band spectrum. The E_F was decided from the Fermi edge of the Au foil loaded on the same sample holder. The E_F was apart by 3.0 eV from the

TABLE I. Change of Ga/N atomic ratio. The numbers in parentheses imply ammonia flow rates in sccm.

Sample	Ga/N ratio
GaN nanowires (100)	1
(Ga,Mn)N nanowires (100)	0.90
(Ga,Mn)N nanowires (150)	0.77

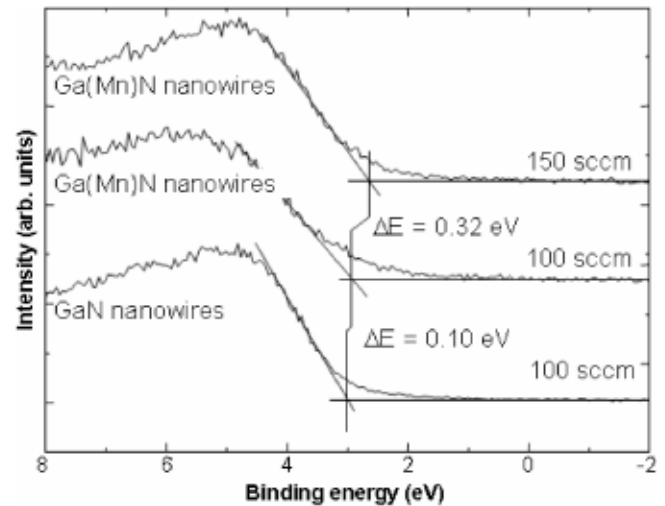


FIG. 5. Change of valence band spectra for (Ga,Mn)N nanowires with ammonia flow rates of 50, 100, and 150 sccm.

VBM for the GaN nanowires. This showed that the nanowires are n -type properties because the band gap of wurtzite GaN is about 3.44 eV. As Mn atoms were incorporated into GaN nanowires, the Fermi level shifted about 0.10 eV toward the VBM in comparison with the GaN nanowires. Mn impurities in GaN act as deep acceptors for electrons.¹ The electron density decreased with increasing Mn doping concentration to the GaN nanowires, resulting in the shift of the Fermi level toward the VBM. When ammonia flow rate increased to 150 sccm, the Fermi level shifted about 0.32 eV toward the VBM. This means that net hole concentration increased due to the increase of number of Ga-vacancies, consistent with the change of Ga/N ratio in Table I.

The observed weak ferromagnetic behaviors of the (Ga,Mn)N nanowires could arise from the formation of nanosized Ga-Mn and Mn-N compounds in (Ga,Mn)N DMS. In the previous work,¹³ a weak ferromagnetism was found below 100 K in a Mn_3Ga bulk material. The Mn_4N showed a ferromagnetic property at temperatures higher than 300 K.¹⁴ In the Mn-implanted GaN,¹² Mn-Ga and Ga-Mn bonds were found in Mn $2p$ and Ga $3d$ spectra, respectively. This means the production of a binary phase of Ga-Mn, playing a role to producing ferromagnetic properties. Meanwhile, no chemical bonding of the Ga-Mn magnetic phase was observed in the GaN nanowire, as shown in Fig. 4. No second phases were also found in HRTEM image [Fig. 1]. From these results, it was concluded that the ferromagnetic properties of the (Ga,Mn)N nanowires were due to a solid solution of Mn ions in GaN, not the nanosized Ga-Mn and Mn-N compounds.

The magnetic moment and Curie temperature of (Ga,Mn)N nanowires increased with increasing ammonia flow rate, as seen in Fig. 2. The enhancement of magnetic properties could be explained with the SRPES results in Figs. 4 and 5. The decrease in Ga/N ratio with the increase of ammonia flow rate means that the concentration of Ga-vacancies increased. This was evident by the shift of Fermi

level toward the VBM with increase of ammonia flow rate in Fig. 5. Incorporation of Mg in GaN significantly depends on the stoichiometry of the growth surface.¹⁵ Mg concentration in GaN increases with an increase of the number of Ga vacancies because the Mg is incorporated into substitutional Ga sites.¹⁶ Similarly, in the growth of (Ga,Mn)N nanowires, Mn ions can also occupy at Ga vacancies,¹ resulting in the increase of Mn concentration, as shown in Mn $2p$ spectra of Fig. 4(a). The Mn atoms occupying Ga sites in (Ga,Mn)N magnetic semiconductors provide the localized spins.¹ Meanwhile, the nanowires showed n -type properties, meaning that the observed ferromagnetic properties might be related to electrons, not to holes. This could be explained by the bound magnetic polaron model.¹⁷ Therefore, the enhancement of ferromagnetic properties in (Ga,Mn)N nanowires with increasing ammonia flow rate originated from the increase of Mn concentration dissolving in GaN.

IV. CONCLUSION

n -type (Ga,Mn)N nanowires were grown on sapphire substrates by a chemical vapor deposition using a mixture of Ga and MnCl_2 powders and ammonia gas. No secondary magnetic phases were found in the nanowires. This supports that the solid solution of Mn ions in GaN nanowires played a major role in producing the ferromagnetic properties. Mn concentration dissolving in GaN and Ga vacancies simultaneously increased with increasing ammonia flow rate, resulting in the increases of ferromagnetic signal and Curie temperature. These (Ga,Mn)N nanowires will offer opportunities for investigations of fundamental science and be very useful in the development of future nanoscale spintronic semiconductor devices.

ACKNOWLEDGMENTS

This work was supported in part by the Korea Science and Engineering Foundation through the Quantum-functional

Semiconductor Research Center at Dongguk University in 2004 and in part by the project for "National Research Laboratory" sponsored by the Korea Institute of Science and Technology Evaluation and Planning (KISTEP). High-resolution XRD and SRPES using synchrotron radiation were carried out at the 3C2 and 8A1 SPEM beamlines at Pohang Accelerator Laboratory (PAL), respectively.

¹H. Munekata, A. Zaslavsky, P. Fumagalli, and R. J. Ganbino, *Appl. Phys. Lett.* **63**, 2929 (1993).

²M. Zajac, R. Doradziński, J. Gosk, J. Szczytko, M. Lefeld-Sosnowska, M. Kamińska, A. Twardowski, M. Palczewska, E. Grzanka, and W. Gebicki, *Appl. Phys. Lett.* **78**, 1276 (2001).

³J. M. Baik and J.-L. Lee, *Met. Mater. Int.* **10**, 555 (2001).

⁴S. Sonoda, S. Shimizu, T. Sasaki, Y. Yamamoto, and H. Hori, *J. Cryst. Growth* **237/239**, 1358 (2002).

⁵T. Dietl, H. Ohno, F. Matsukura, J. Cibert, and D. Ferrand, *Science* **287**, 1019 (2000).

⁶T. Szyszko, G. Kamler, B. Strojek, G. Weisbrod, S. Podsiadło, L. Adamowicz, W. Gębicki, J. Szczytko, A. Twardowski, and K. Sikorski, *J. Cryst. Growth* **233**, 631 (2001).

⁷M. L. Reed, N. A. El-Masry, H. H. Stadelmaier, M. K. Ritums, M. J. Reed, C. A. Parker, J. C. Roberts, and S. Bedair, *Appl. Phys. Lett.* **79**, 3473 (2001).

⁸M. van Schilfgaarde and O. N. Mryasov, *Phys. Rev. B* **63**, 233205 (2001).

⁹K. Sato and H. Katayama-Yoshida, *Jpn. J. Appl. Phys., Part 2* **40**, L485 (2001).

¹⁰H. Katayama-Yoshida, R. Kato, and T. Yamamoto, *J. Cryst. Growth* **231**, 428 (2001).

¹¹W. Q. Han and A. Zettl, *Appl. Phys. Lett.* **80**, 303 (2002).

¹²J. M. Baik, H. W. Jang, J. K. Kim, and J.-L. Lee, *Appl. Phys. Lett.* **82**, 583 (2003).

¹³H. Niida, T. Hori, and Y. Nakagawa, *J. Phys. Soc. Jpn.*, **52**, 1512 (1983).

¹⁴H. Nakayama, H. Mashita, Erkin Kulatov, R. Funahashi, and H. Ohta, *J. Magn. Magn. Mater.*, **258**, 323 (2003).

¹⁵B. Schineller, A. Gutzzeit, P. H. Lim, M. Schwambersa, K. Heime, O. Schön and M. Heuken, *J. Cryst. Growth* **195**, 274 (1998).

¹⁶J. W. Orton, C. T. Foxon, T. S. Cheng, S. E. Hooper, S. V. Novikov, B. Ya. Ber, and Yu. A. Kudriavtsev, *J. Cryst. Growth* **197**, 7 (1999).

¹⁷A. C. Durst, R. N. Bhatt, and P. A. Wolff, *Phys. Rev. B* **65**, 235205 (2002).